AIMS Biophysics, 4(1): 90-106.
DOI: 10.3934/biophy.2017.1.90
Received: 06 October 2016
Accepted: 22 January 2017
Published: 06 February 2017

http://www.aimspress.com/journal/biophysics

Research article

Plant potassium channels are in general dual affinity uptake systems

Ingo Dreyer *

Centro de Bioinformática y Simulación Molecular, Facultad de Ingeniería, Universidad de Talca, Talca, Chile

*** Correspondence:** Email: idreyer@utalca.cl; Tel: +56-71-2418975.

Abstract: In plant science, we are currently at the dawn of an era, in which mathematical modeling and computational simulations will influence and boost tremendously the gain of new knowledge. However, for many plant scientists mathematical modeling is still rather dubious and is often negligently considered as an oversimplification of the real situation. The goal of this article is to provide a toolbox that allows first steps in the modeling of transport phenomena in plants. The provided framework is applied in the simulation of K^+ uptake by cells via K^+ channels. Historically, K^+ uptake systems are divided into "high affinity" (e.g. H^+-coupled K^+ transporters) and "low affinity" (K^+ channels) transporters. The computational cell biology studies presented here refute this separation. They show that K^+ channels are in general uptake systems with "low" and "high affinity" components. The analyses clarify that constraints in wet-lab experiments usually mask the "high affinity" component. Consequently, the channels were widely assigned a "low affinity" component, only. The results presented here unmask the absurdity of the concept of "high- and low-affinity" transporters.

Keywords: ion channels; computational cell biology; transport; membrane; mathematical modeling

1. Introduction

The goal of biophysics is to provide a comprehensive theory, based on fundamental laws and/or first principles, that allows to explain experimental findings in biological experiments and to express the findings in numbers. Lord Kelvin once stated: *"When you cannot express [a finding] in numbers, your knowledge is of a meagre and unsatisfactory kind; it may be the beginning of knowledge, but you have scarcely in your thoughts advanced to the state of Science."* In this context, we may

consider biophysics, with some degree of arrogance, as the core of biological science. This would be certainly an exaggeration; nevertheless, we should not underestimate the power of mathematical descriptions of biological phenomena; in particular, because the mathematical description of the different entities of a complex system allows to reassemble the system in a computer and enables then to simulate its behavior.

In plant science we are currently at the dawn of an era, in which computational simulations will influence and boost tremendously the gain of new knowledge. An advanced field in this context is the area of membrane transport, simply because scientists in this area are forced to work since decades with biophysical and mathematical approaches; otherwise these transport processes would be hard to grasp. Meanwhile a couple of models for coupled transport processes enabled already far reaching insights. There are models, for instance, for electrical signaling [1,2,3], guard cells [4,5], phloem re-loading [6], salt stress [7] or nutrient exchange in arbuscular mycorrhizal symbiosis [8].

The goal of the study presented here is to provide a toolbox that allows first steps in the modeling of transport phenomena in plants and other organisms. On the basis of an example, it is explained how the biophysical basis of transmembrane transport can be described in mathematical terms. The chosen example is the H^+-ATPase-driven uptake of K^+ via potassium channels. Potassium channels and transporters are historically separated in "high affinity" and "low affinity" uptake systems [9], whereby K^+ channels were assigned as "low affinity" systems. The computational simulations of this study reveal that the separation according to the apparent affinity is a historic fallacy. It is shown that K^+ channels are in general uptake systems with "low" and "high affinity" components. Both components are intrinsic properties of the uptake mechanism. The features of K^+ channels, however, in particular their high turnover rate, complicate the detection of the "high affinity" component in wet-laboratory experiments. Consequently, the channels were historically assigned a "low affinity" component, only.

2. Materials and Methods

2.1. Current through an open ion channel

An ion channel is a diffusion facilitator. It mediates the selective transport of ions along a transmembrane electrochemical gradient. In its general form, the current through N open ion channels of a certain type is determined by the equation

$$I(V) = N \cdot z \cdot e_0 \cdot j \cdot A \qquad \text{(eqn. 2.1.1)}$$

where z determines the valence of the ion, $e_0 \approx 1.602 \times 10^{-19} C$ the elementary charge, A the surface of a cross-section of the ion channel, and j the flux density of ions per second per surface unit. The driving force of j originates from a gradient in the electrochemical potential μ:

$$\mathrm{j} = -\mathrm{K} \cdot [\mathrm{c}] \cdot \nabla\mu \qquad \text{(eqn. 2.1.2)}$$

with K being a proportional coefficient and

$$\mu = \mu^0 + \mathrm{RT} \cdot \ln\frac{[\mathrm{c}]}{[\mathrm{c_0}]} + \mathrm{z} \cdot \mathrm{F} \cdot \psi \qquad \text{(eqn. 2.1.3)}$$

Here, $[c]$ is the concentration distribution of the permeating ion, $[c_0]$ an arbitrary reference concentration, ψ the electric potential, F the Faraday constant, R the gas constant and T the absolute temperature. For an ion channel, the gradient is essentially in one direction, only, namely along the permeation pathway. Therefore, eqn. 2.1.2 can be expressed in one dimension resulting in the Nernst-Planck equation:

$$\mathrm{j} = -\mathrm{D} \cdot \left(\frac{\partial}{\partial \mathrm{x}} [\mathrm{c}] + \frac{\mathrm{zF}}{\mathrm{RT}} \cdot [\mathrm{c}] \cdot \frac{\partial}{\partial \mathrm{x}} \psi \right) \qquad \text{(eqn. 2.1.4)}$$

with the diffusion coefficient of the ion $D = K \cdot RT$. As outlined in Hille [10], the differential eqn. 2.1.4 can be multiplied on both sides by the factor $\frac{1}{D} \cdot e^{\frac{zF}{RT}\psi}$ and integrated, resulting in

$$\mathrm{j} = \frac{\mathrm{c_{ext}} - \mathrm{c_{int}} \cdot \mathrm{e}^{\frac{\mathrm{zF}}{\mathrm{RT}} \cdot \mathrm{V}}}{\int_0^1 \frac{1}{\mathrm{D(x)}} \cdot \mathrm{e}^{\frac{\mathrm{zF}}{\mathrm{RT}} \cdot \psi(\mathrm{x})} \mathrm{dx}} \qquad \text{(eqn. 2.1.5)}$$

Here, x denotes the fraction across the membrane from inside the cell ($x = 0$) to the outside ($x = 1$); $\psi(1) = \psi_{ext} = 0$, $\psi(0) = \psi_{int} = V$, $[c](1) = c_{ext}$, $[c](0) = c_{int}$. With the assumptions (Figure 1A) (i) that the diffusion coefficient is constant across the membrane: $D(x) = D = const.$, and (ii) that the transmembrane potential varies linearly across the membrane: $\psi(x) = \psi_{int} - x \cdot (\psi_{int} - \psi_{ext})$, the denominator of eqn. 2.1.5 can be integrated resulting in the well-known Goldman-Hodgkin-Katz (GHK) flux equation:

$$\mathrm{j} = \mathrm{D} \cdot \frac{\mathrm{zF}}{\mathrm{RT}} \cdot \mathrm{V} \cdot \frac{\mathrm{c_{int}} - \mathrm{c_{ext}} \cdot \mathrm{e}^{-\left(\frac{\mathrm{zF}}{\mathrm{RT}} \cdot \mathrm{V}\right)}}{1 - \mathrm{e}^{-\left(\frac{\mathrm{zF}}{\mathrm{RT}} \cdot \mathrm{V}\right)}} \qquad \text{(eqn. 2.1.6)}$$

However, at least for potassium channels, it is known that these conditions are not fulfilled. The internal cavity of the channel and the selectivity filter cause that neither the diffusion coefficient is constant nor that the transmembrane potential varies linearly. Thus, for plant K^+ channels the GHK-flux equation is wrong. Instead, the following relations approximate the conditions in K^+ uptake channels (Figure 1B): (i) in the region between $x = 0$ and $x = a$: $[c](x) = c_{int}$, $D(x) = D_s$ and $\psi(x) = \psi_{int} = V$; (ii) in the interval between $x = a$ and $x = b$: $\psi(x) = \psi_{int} - \frac{x-a}{b-a} \cdot (\psi_{int} - \psi_{ext})$ and $D(x) = D$; and (iii) in the region between $x = b$ and $x = 1$: $[c](x) = c_{ext}$, $D(x) = D_s$ and $\psi(x) = \psi_{ext} = 0$; with $0 \leq a < b \leq 1$; D_s is the diffusion coefficient of the ion in free solution and D the diffusion coefficient in the narrow pore.

Following step-wise integration of the denominator in eqn. 2.1.5, it results:

$$\mathrm{j} = \frac{\mathrm{D}}{\mathrm{b-a}} \cdot \frac{\mathrm{zF}}{\mathrm{RT}} \cdot \mathrm{V} \cdot \frac{\mathrm{c_{int}} - \mathrm{c_{ext}} \cdot \mathrm{e}^{-\left(\frac{\mathrm{zF}}{\mathrm{RT}} \cdot \mathrm{V}\right)}}{1 - \mathrm{e}^{-\left(\frac{\mathrm{zF}}{\mathrm{RT}} \cdot \mathrm{V}\right)} + \frac{\mathrm{zF}}{\mathrm{RT}} \cdot \mathrm{V} \cdot \frac{\mathrm{D}}{\mathrm{D_S}} \cdot \left(\frac{\mathrm{a}}{\mathrm{b-a}} + \frac{1-\mathrm{b}}{\mathrm{b-a}} \cdot \mathrm{e}^{-\left(\frac{\mathrm{zF}}{\mathrm{RT}} \cdot \mathrm{V}\right)} \right)} \qquad \text{(eqn. 2.1.7)}$$

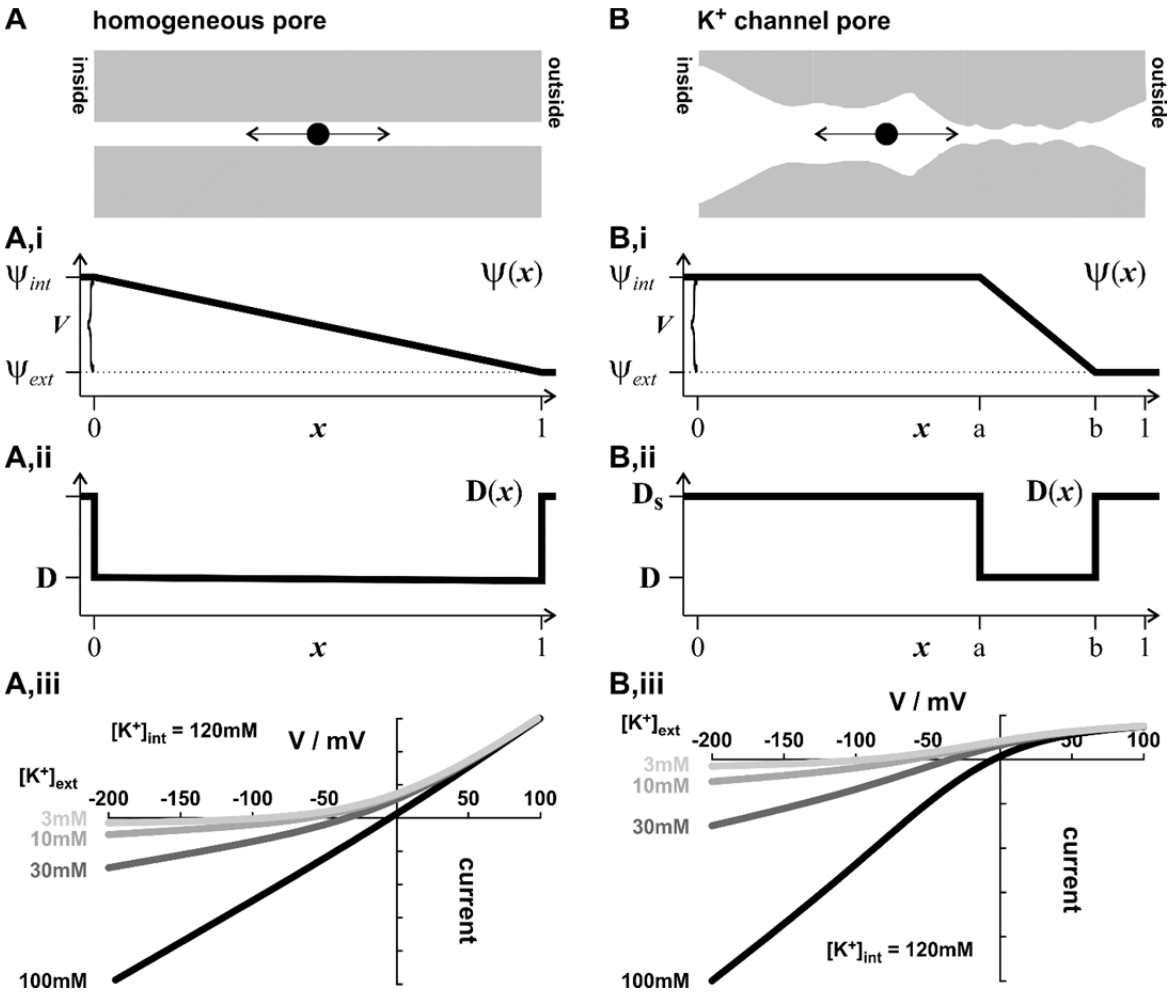

Figure 1. Comparison of the current through a homogenous pore and a structured K^+ channel pore. (A) In a homogenous pore, the transmembrane potential difference drops linearly across the membrane (A,i) and the diffusion coefficient is constant over the entire distance but lower than in free solution (A,ii). (A,iii) Current voltage curves of a model cell with only homogeneous K^+ selective ion channels and an internal potassium concentration of $[K^+]_{int}$ = 120 mM calculated according to eqn. 2.1.6. Please note that all curves for $[K^+]_{ext} < [K^+]_{int}$ are left-bended, which contradicts experimental findings for plant K^+ uptake channels. (B) The pore of plant K^+ uptake channels has an internal structure as resolved by homology modeling using the crystal structures of mammalian K^+ channels as template [6,11–15]. Open K^+ channels have in general an internal cavity that is connected to the inside of the cell. In this cavity the electric potential (B,i for x = 0…a) can be approximated to be identical to the potential inside the cell and the diffusion coefficient for K^+ (D_s) is as in free solution (B,ii for x = 0…a). The narrow selectivity filter is the main obstacle for the passage of the ion. Here, the transmembrane potential difference drops across a short distance (B,i for x = a…b) and the diffusion coefficient (D) is smaller (B,ii for x = a…b). Beyond the selectivity filter (x = b…1) the conditions are as in free solution outside the cell. The conditions of plant K^+ channels are well described with a = 0.75, b = 1, and D/D_s = 0.25. (B,iii) The current voltage curves were determined according to eqn. 2.1.9 and coincide very well with previously published experimental data.

With the parameters $a \approx 0.75$, $b \approx 1$, $\frac{D}{D_s} \approx 0.25$, the flux equation describes quite well the experimentally measured currents mediated by open K^+ uptake channels with right-bended curves at moderate $[K^+]_{ext}$ (Figure 1B; [16–29]):

$$j_K = \frac{D}{0.25} \cdot \frac{zF}{RT} \cdot V \cdot \frac{c_{int} - c_{ext} \cdot e^{-\left(\frac{zF}{RT} \cdot V\right)}}{1 - e^{-\left(\frac{zF}{RT} \cdot V\right)} + 0.75 \cdot \frac{zF}{RT} \cdot V} \qquad \text{(eqn. 2.1.8)}$$

With this equation and with $\frac{RT}{F} \approx 25mV$, the voltage and concentration dependence of the current through N open potassium channels can be expressed as

$$I_{open\,K}(V) = \sigma_K \cdot \frac{1}{mV \cdot \mu M} \cdot V \cdot \frac{[K^+]_{int} - [K^+]_{ext} \cdot e^{-\left(\frac{V}{25mV}\right)}}{1 - e^{-\left(\frac{V}{25mV}\right)} + 0.75 \cdot \frac{V}{25mV}} \qquad \text{(eqn. 2.1.9)}$$

with the conductance σ_K being proportional to the number of channels. This approximation simplifies the uncertainty of several microscopic parameters to one macroscopic parameter, σ_K, that can easily be adjusted using experimental values or can be screened in simulations in a reasonable parameter interval. Also in case of eqn. 2.1.9 the zero-current potential V_{rev}, at which $I_{Open\_K}(V_{rev}) = 0$, depends on the external and internal potassium concentrations and is determined by the Nernst-equation:

$$V_{rev} = \frac{RT}{F} \cdot \ln \frac{[K^+]_{ext}}{[K^+]_{int}} \qquad \text{(eqn. 2.1.10)}$$

2.2. Current through a voltage-gated ion channel

In the previous section the voltage dependence of the permeation of ions through an open channel was considered. This, however, is not the normal situation in a cellular context. Usually, an ion channel is not open all the time, but its activity is regulated by external stimuli, as, for instance, the membrane voltage or the concentration of a ligand. The following example of a voltage-gated ion channel illustrates, how such a dependency of the channel activity on an external parameter can be described in simple mathematical expressions.

A channel protein can exist in different conformations; in the simplest case in two (Figure 2): the open state that allows ions to permeate as described in section 2.1. and the closed state that does not permit ions to pass the channel. The different conformation states are correlated with different energetic statuses of the protein. In the open state, the channel protein is characterized by the free energy G_O and in the closed state by G_C. For transitions O ↔ C the channel has to go through an instable intermediate state P with the energy peak G_P. The channel has to overcome the energy barrier $\Delta G_{PO} = G_P - G_O$ when changing from the open into the closed state and the energy barrier $\Delta G_{PC} = G_P - G_C$ when changing from the closed into the open state. The transitions between the states can be described by the rates a (activation; O → C) and d (deactivation; C → O). With these rates the changes in the number of open (N_O) or closed (N_C) channels in the small time-interval dt can be calculated:

$$\begin{cases} dN_O = dt \cdot (-d \cdot N_O + a \cdot N_C) \\ dN_C = dt \cdot (\ \ d \cdot N_O - a \cdot N_C) \end{cases} \qquad \text{(eqn. 2.2.1)}$$

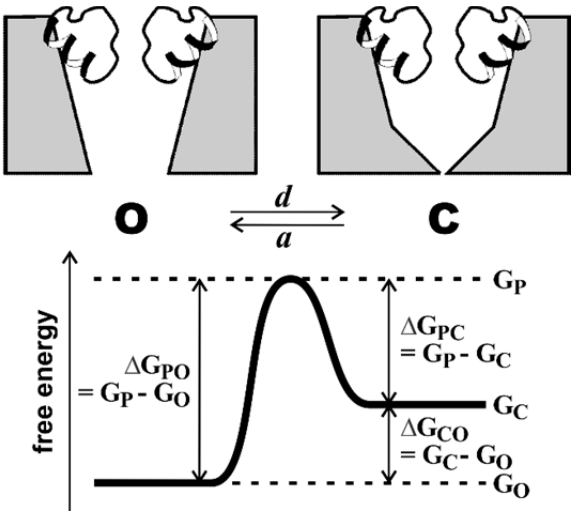

Figure 2. State model of an ion channel that can exist either in the open or in the closed conformation. Each conformation is characterized by a specific free energy (G_O and G_C, respectively). A conformational change implies a change of the energy status, whereby the energy barrier that has to overcome is determined by an instable intermediate conformation (G_P). Mathematically, the transitions can be described by the rates *a* (activation; C → O) and *d* (deactivation; O → C). Figure modified from Dreyer et al., 2004 [30]

By dividing eqn. 2.2.1 by the total number of channels, $N = N_O + N_C$, it results an equation system that determines the probabilities to find a channel in the open and in the closed conformation, p_O and p_C, respectively; written in matrix-form:

$$d\begin{pmatrix} p_O \\ p_C \end{pmatrix} = dt \cdot \begin{pmatrix} -d & a \\ d & -a \end{pmatrix} \cdot \begin{pmatrix} p_O \\ p_C \end{pmatrix} \qquad \text{(eqn. 2.2.2)}$$

generally written:

$$d\vec{p} = dt \cdot \boldsymbol{Q} \cdot \vec{p}$$

with the vector $\vec{p}$ and the so-called $\boldsymbol{Q}$-Matrix. The matrix form is not needed in this simple example. However, it is rather useful, if a protein can exist in more than two states. An entire toolbox from linear algebra can be applied to such equation systems.

According the Eyring rate theory [31], the rates *a* and *d* are correlated with the height of the respective energy barrier (Figure 2):

$$a = \frac{kT}{h} \cdot e^{-\left(\frac{\Delta G_{PC}}{kT}\right)} = \frac{kT}{h} \cdot e^{-\left(\frac{G_P - G_C}{kT}\right)} \qquad \text{(eqn. 2.2.3)}$$

$$d = \frac{kT}{h} \cdot e^{-\left(\frac{\Delta G_{PO}}{kT}\right)} = \frac{kT}{h} \cdot e^{-\left(\frac{G_P - G_O}{kT}\right)} \qquad \text{(eqn. 2.2.4)}$$

with the Boltzmann constant k, the Planck constant h and the absolute Temperature T. If we now consider eqn. 2.2.2 in the case of thermal equilibrium, the differential equation simplifies to a linear equation system because in equilibrium there is no change in the probabilities to find a channel in the open or the closed conformation ($dp_O/dt = dp_C/dt = 0$). Using additionally the fact that the probability to find the channel in any of the two states is 1 ($p_O + p_C = 1$), it can be derived:

$$p_{Oss} = \frac{a}{a+d} = \frac{1}{1+e^{\left(\frac{G_O - G_C}{kT}\right)}} \qquad \text{(eqn. 2.2.5)}$$

$$p_{Css} = \frac{d}{a+d} = \frac{1}{1+e^{\left(\frac{G_C - G_O}{kT}\right)}} \qquad \text{(eqn. 2.2.6)}$$

Here p_{Oss} and p_{Css} denote the steady state probabilities to find the channel in the open and the closed conformation, respectively. Functions like eqn. 2.2.5 and 2.2.6 are often called "Boltzmann functions" of the channel, because they also result from Boltzmann-statistics, which correlates the probabilities of two states in thermal equilibrium with the energy difference between these states:

$$\frac{p_{Oss}}{p_{Css}} = e^{-\left(\frac{G_O - G_C}{kT}\right)} \qquad \text{(eqn. 2.2.7)}$$

Eyring rate theory and Boltzmann statistics provide general tools to describe conformational changes of a channel protein. The eqns. 2.2.1–2.2.7 do not contain any dependency on the voltage or any other parameter that may have a modulatory effect on the channel. For a voltage-gated channel, the question is now: *How does the voltage dependence come into play?* The answer is: The energy levels G_O, G_C, and G_P depend on the membrane voltage V in the case of a voltage-gated channel or on a ligand concentration in the case of a ligand-gated channel. Unfortunately, the exact relationship of neither $G_O(V)$, $G_C(V)$, nor $G_P(V)$ is known. But, this detailed information is not necessary; instead, the voltage dependence can be deduced by the Taylor approximation of $G(V)$. Usually, the first order Taylor approximation is sufficient to describe the dependence in the physiologically relevant voltage interval:

$$G(V) \approx G_0 + Q \cdot V \qquad \text{(eqn. 2.2.8)}$$

where $G_0 = G(0)$ has the dimension of an energy and $Q = G'(0)$ the dimension of a charge. Using eqn. 2.2.8, the rates $a(V)$, $d(V)$ and the steady state open probability $p_{Oss}(V)$ in eqns. 2.2.4–2.2.5 can be expressed after further simplification and combination of redundant parameters as:

$$a(V) = \frac{1}{s} \cdot e^{\left(a_0 + a_V \cdot \frac{V}{25mV}\right)} \qquad d(V) = \frac{1}{s} \cdot e^{\left(d_0 + d_V \cdot \frac{V}{25mV}\right)} \qquad p_{Oss}(V) = \frac{1}{1+e^{\left((d_0 - a_0) + (d_V - a_V) \cdot \frac{V}{25mV}\right)}}$$

with the dimensionless parameters a_0, d_0, a_V, and d_V.

The current through a voltage-gated ion channel can be described by the current through the open channel multiplied with the probability to find the channel open, $p_O(V)$:

$$I_{V-gated\ channel}(V) = I_{open\ channel}(V) \cdot p_O(V) \qquad \text{(eqn. 2.2.9)}$$

Figure 3 shows three different steady state current voltage curves that were all generated with eqn. 2.2.9. Figure 3A represents inward-rectifying plant K^+ channels, Figure 3B outward-rectifying

plant K^+ channels [32,33] and Figure 3C voltage-gated organic acid channels in guard cells [34]. Although the three curves look fundamentally different, they all have the same biophysical bases.

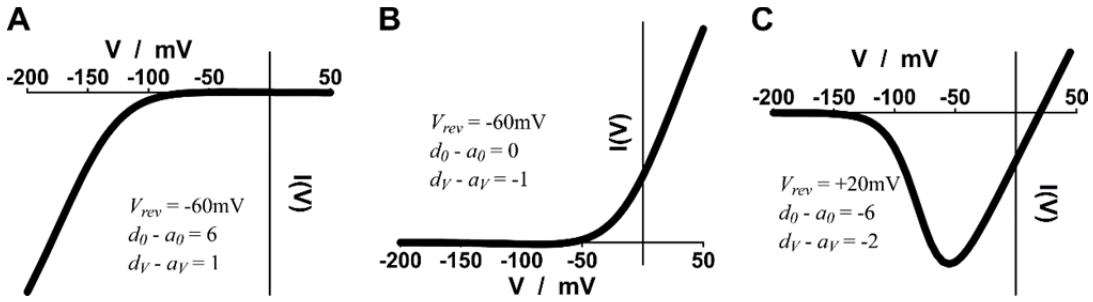

Figure 3. Computational simulation of currents through voltage-gated ion channels. All three curves were generated with eqn. 2.2.9 using the indicated parameters. (A) Current voltage characteristic of inward-rectifying K^+ channels. (B) Current voltage characteristic of outward-rectifying K^+ channels. (C) Current voltage characteristic of organic acid channels of the QUAC-type. $V_{rev} = \frac{RT}{zF} \cdot \ln \frac{c_{ext}}{c_{int}}$.

2.3. A model for the H^+-ATPase

For the computational simulations of potassium uptake (next section) we also need a mathematical model of the "power plant" of transmembrane transport in plants, the H^+-ATPase. Figure 4A illustrates the stepwise mechanism of the pump cycle. This mechanistic model can be mathematically represented by an equation similar to eqn. 2.2.2 but with a 6 × 6 ***Q***-matrix. Further linear algebra details, however, would go far beyond the scope of this article. Therefore, we content ourselves here with the final equation that describes the current flow mediated by the pump:

$$I_{pump}(V) = I_{max} \cdot \frac{1-e^{-\left(\frac{V}{25mV}+A\right)}}{1+e^{-\left(\frac{V}{25mV}+B\right)}+e^{-\left(D\cdot\frac{V}{25mV}+C\right)}} \qquad \text{(eqn. 2.3.1)}$$

The parameter D is a number between 0 and 1, while the parameters I_{max}, A, B, and C depend in a complicated manner on the internal and external proton concentrations and on the cytosolic ATP and ADP concentrations. Under "normal" conditions in simulations, strong fluctuations in these concentrations are not expected. In this case, A, B, and C are just numbers and modifications in I_{max} can represent altered activities of the pump. Based on experimental data, a suitable mathematical representation of the pump current was found as [6] (Figure 4B):

$$I_{pump}(V) = I_{max} \cdot \frac{1-e^{-\left(\frac{V+250mV}{25mV}\right)}}{1+e^{-\left(\frac{V}{25mV}+8\right)}+e^{-\left(0.32\cdot\frac{V}{25mV}+2.5\right)}} \qquad \text{(eqn. 2.3.2)}$$

2.4. Computational simulation of potassium uptake using K^+ channels

After having derived the mathematical representations of pumps and channels, this knowledge can now be employed in computational cell biology approaches. As an example, we consider the H^+-ATPase-driven uptake of K^+ by a cell via inward-rectifying K^+ (Kin) channels (Figure 5).

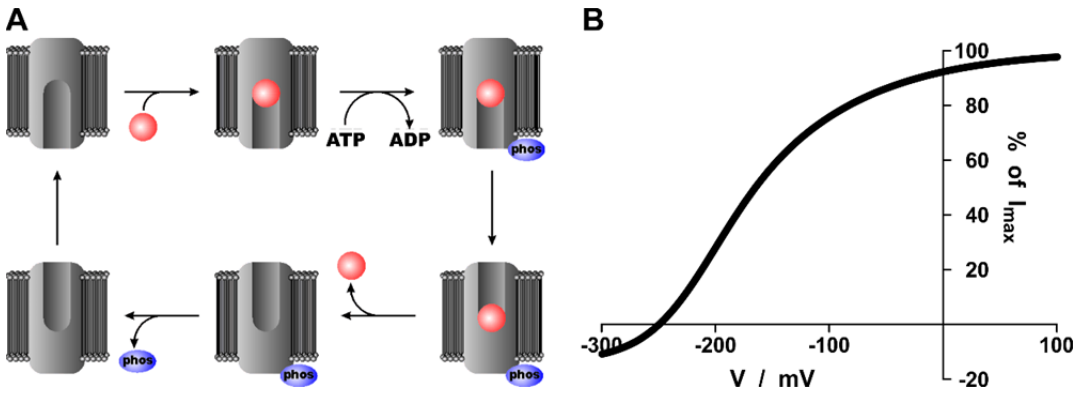

Figure 4. The plasma membrane H^+-ATPase. (A) Mechanistic model illustrating the different steps of the pump cycle. Starting on top-left and then continuing clockwise: A proton from the internal medium binds to the protein. By using the energy from ATP-hydrolysis the protein gets phosphorylated. The phosphorylated protein with the proton bound is less stable and undergoes a conformational change that provides access of the proton to the external medium and that reduces the affinity of the proton to the protein. The proton dissociates and the phosphate gets cleaved off. The protein without phosphate and proton is more stable in the initial conformation. The cycle can start again. (B) Mathematical description of the pump current using eqn. 2.3.2. Please note that in this case the zero-current potential V_{rev}, at which $I_{pump}(V_{rev}) = 0$, is $V_{rev} = -250$ mV.

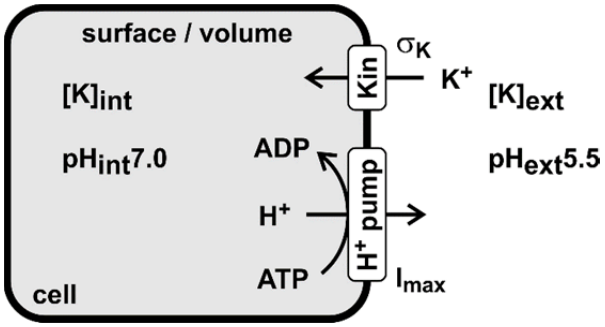

Figure 5. *In silico* cell to study K^+ uptake. The membrane of the *in silico* cell contains two transporter types: proton ATPase (H^+ pump) and inward-rectifying K^+ channel (Kin). Each transporter type is represented by one free parameter σ_K and I_{max}, respectively that describe their activity (expression level). The cell is characterized by surface and volume. The relevant concentrations for the model cell are the internal and external potassium and proton concentrations. To reflect the proton-buffer capacities in the cell and in the extracellular medium (usually buffered in uptake experiments by chemical buffers), the pH values were kept constant at $pH_{int} = 7.0$ and $pH_{ext} = 5.5$.

The voltage-dependence of the H^+-ATPase was mathematically described as shown in Figure 4B:

$$I_{pump}(V) = I_{max} \cdot \frac{1-e^{-\left(\frac{V+250mV}{25mV}\right)}}{1+e^{-\left(\frac{V}{25mV}+8\right)}+e^{-\left(0.32\cdot\frac{V}{25mV}+2.5\right)}} = I_{max} \cdot f_H(V) \qquad \text{(eqn. 2.4.1)}$$

and that of the Kin channel as shown in Figure 3A. Because the voltage changes at the membrane of the cell is much slower than the relaxation of the Kin channel gate, no further relaxation kinetics (separated description of $a(V)$ and $d(V)$) needed to be taken into account resulting in the equation of the voltage-dependent current through Kin channels:

$$I_{Kin}(V) = \sigma_K \cdot \frac{V}{mV} \cdot \frac{\frac{[K^+]_{int}}{\mu M} - \frac{[K^+]_{ext}}{\mu M}\cdot e^{-\left(\frac{V}{25mV}\right)}}{1-e^{-\left(\frac{V}{25mV}\right)}+0.75\cdot\frac{V}{25mV}} \cdot \frac{1}{1+e^{\left(\frac{V}{25mV}+6\right)}} = \sigma_K \cdot i_K(V) \qquad \text{(eqn. 2.4.2)}$$

The system is fully determined by the following parameters/variables: volume, surface, current or conductance of the two transporter types (I_{max} [H^+ pump], σ_K [Kin]), concentrations $[K]_{int}$, $[K]_{ext}$, $[H]_{int}$, $[H]_{ext}$, and the membrane voltage. To reflect the pH buffer capacities, the internal and external pH-values were set constant to pH_{ext} = 5.5 ($[H]_{ext}$ = 3.16 μM) and pH_{int} = 7.0 ($[H]_{int}$ = 0.1 μM).

Generally, the transport of K^+ across the membrane is accompanied by the transport of a counterion, e.g. Cl^-. *Why does the model do not contain the counterion transport?* The answer is simple. (i) We consider for K^+ uptake only a small time-scale, in which osmotic effects can be neglected. (ii) The uptake of Cl^- ions is coupled to the proton gradient and is either electroneutral as an 1:1 H^+/Cl^- co-transport or an electrogenic 1:X H^+/Cl^- co-transport with X > 1 that is electrically compensated by the export of protons via the pump. To keep the focus on the essentials of the model (the initial dynamics of K^+ uptake), all these background aspects of the counterion transport can be implicitly gathered in $I_{pump}(V)$.

The H^+-ATPase-driven K^+ uptake under controlled conditions is determined by the following iteration:

(1) Pre-set $[K]_{ext}$
(2) t = 0 s; set start value for $[K]_{int}$
(3) Determine $V_0 = V(0)$ using the relation $I_{max} \cdot f_H(V_0) = \sigma_K \cdot i_K(V_0)$
(4) Calculate $d[K]_{int} = dt \cdot \frac{1}{volume} \cdot \sigma_K \cdot \frac{-i_K(V)}{e_0}$
(5) Calculate $dV = dt \cdot \frac{1}{surface \cdot C_M} \cdot [I_{max} \cdot f_H(V) + \sigma_K \cdot i_K(V)]$
(6) Calculate $V(t+dt) = V(t) + dV$
(7) Calculate $[K]_{int}(t+dt) = [K]_{int}(t) + d[K]_{int}$
(8) Move to the next time point $t + dt \rightarrow t$, and repeat the steps from (4)

$C_M \approx 10^{-2}$ pF/μm^2 is the specific capacitance of the membrane. Several of the remaining parameters (volume, surface, σ_K, I_{max}, time) are redundant, *i.e.* the effect of a change in one parameter is identical to the effect of the change in another. Therefore, this parameter set needs to be cleared from these redundancies. By defining (i) the surface to volume ratio $\alpha := \frac{surface}{volume}$, (ii) the

relative conductance-per-surface-unit $\sigma_{K\_rel} \coloneqq \frac{\sigma_K}{surface}$, and (iii) the relative maximal current-per-surface-unit $I_{\max\_rel} \coloneqq \frac{I_{max}}{surface}$, the equations for $d[K]_{int}$ and dV can be further simplified:

(4) $d[K]_{int} = dt \cdot \alpha \cdot \sigma_{K\_rel} \cdot \frac{-i_K(V)}{e_0}$

(5) $dV = dt \cdot \frac{1}{C_M} \cdot \left[I_{\max\_rel} \cdot f_H(V) + \sigma_{K\_rel} \cdot i_K(V)\right]$

resulting in three free parameters (α, I_{max_rel}, and σ_{K_rel}), the influence of which can be evaluated in computational simulations by parameter screening.

The behavior of the transporter network was mathematically simulated using Virtual Cell Modeling and Analysis Software developed by the National Resource for Cell Analysis and Modeling, University of Connecticut Health Center [35].

3. Results

3.1. K^+ uptake experiments with H^+ pump and Kin

In a first approach, the *in silico* cell was simulated with $[K]_{ext}$ = 10 μM and a starting value of $[K]_{int}$ = 1 mM (highly K^+-starved cell) was chosen. Different starting values do not change the results qualitatively. The accumulation of K^+ over time was measured showing that $[K]_{int}$ accumulates until a saturation level at ~ 220 mM is reached. At this level the V_{rev} of the Kin channel is ~ –250 mV, being identical to the V_{rev} of the H^+-ATPase (Figure 4). If there are many Kin channels in the membrane (σ_{K_rel} is large) the equilibrium is reached quicker (Figure 6A, black curve) than with fewer Kin channels (Figure 6A, grey curve). A same behavior is found for I_{max_rel} (Figure 6B) and the surface-to-volume ratio α of the cell (Figure 6C). Because the effects of a change in the three parameters are qualitatively the same, we focus in the following on the parameter σ_{K_rel}. The obtained results can be easily generalized to the other two parameters.

3.2. Simulation of wet-lab experiments

In the next step, the system was challenged by repeating K^+ uptake experiments as they are carried out in wet-laboratories. $[K]_{ext}$ was fixed and the simulation started with $[K]_{int}(0)$ = 1 mM. As in wet-lab experiments at a fixed time point relatively early after starting the experiment, the K^+ flux was measured and plotted in a [K]-flux vs. $[K]_{ext}$ graph. By multiple repetitions, a large range of $[K]_{ext}$ values between 0.1 μM and 20 mM could be scanned resulting in a curve with an apparent saturation behavior (Figure 7A).

From the consensus in current literature, it would be expected that Kin channels are "low affinity" uptake systems and that K^+-uptake curves like Figure 7A could be described by a simple Michaelis-Menten kinetics equation:

$$v = \frac{v_{max} \cdot [K]_{ext}}{K_m + [K]_{ext}} \quad \text{(eqn. 3.2.1)}$$

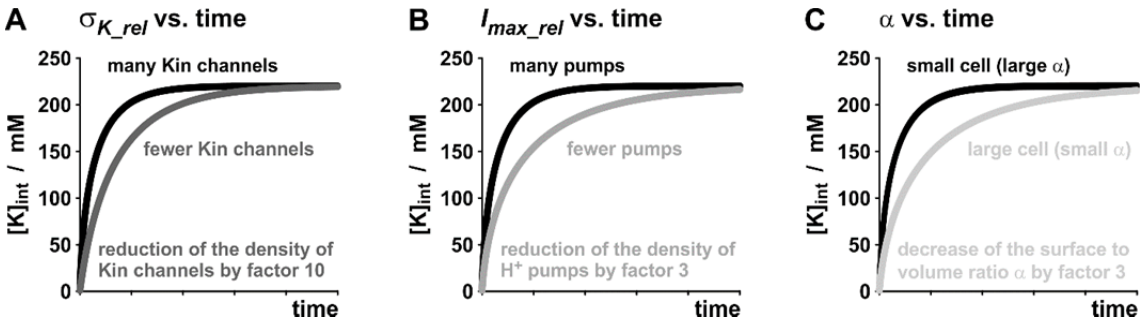

Figure 6. *In silico* cell to study K^+ uptake. Simulation of $[K]_{int}$ accumulation with $[K]_{ext}$ = 10 μM starting from $[K]_{int}(0)$ = 1 mM. (A) Effect of a change in the density of Kin channels on the accumulation time course. A reference simulation (black curve) was repeated but with a ten-fold lower σ_{K_rel} (grey curve). (B) Effect of a change in the density of pumps on the accumulation time course. A reference simulation (black curve) was repeated but with a three-fold lower I_{max_rel} (grey curve). (C) Effect of a change in the cellular surface-to-volume ratio α on the accumulation time course. A reference simulation (black curve) was repeated but with a three-fold smaller value for α (grey curve).

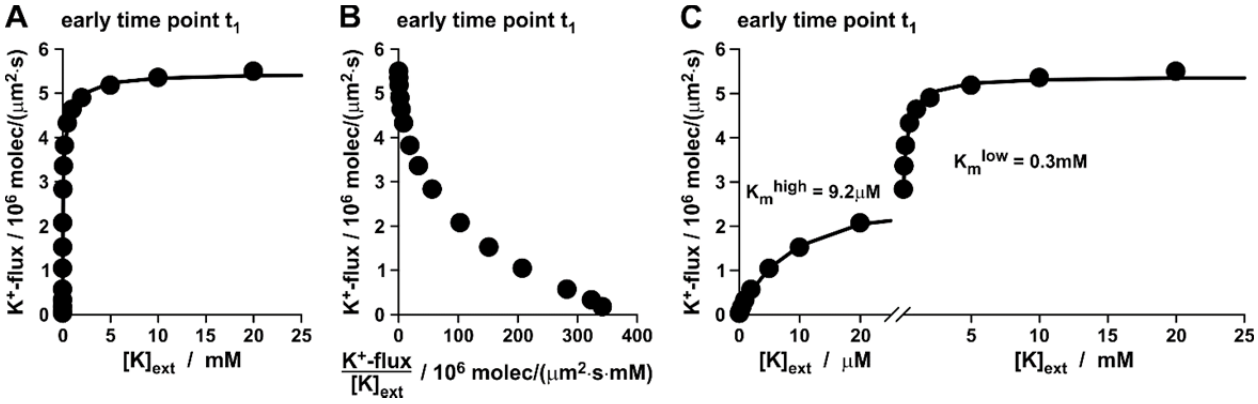

Figure 7. Dual affinity behavior of Kin channels. (A) Rate of K^+ absorption as a function of $[K]_{ext}$ measured at an early time point t_1. (B) Eadie-Hofstee plot of the data from A. The data do not describe a straight line but a sum of at least two lines, one with a steep slope ("low affinity") and another with a moderate slope ("high affinity"). (C) Data from A displayed for two ranges (0–25 μM and 40 μM–25 mM) at different scales. The lines in A, and C represent best fits of the data with eqn. 3.2.2.

However, the data points could not be described by this equation. Instead, it was necessary to use an equation that was developed to describe *two* absorption mechanisms [9] (Figure 7A, line):

$$v = \frac{v_{max} \cdot [K]_{ext}}{K_{m1} + [K]_{ext}} + \frac{v_{max} \cdot [K]_{ext}}{K_{m2} + [K]_{ext}} \qquad \text{(eqn. 3.2.2)}$$

The apparent "dual affinity" of Kin was further corroborated in the Eadie-Hofstee representation of the data (Figure 7B). Here, the data points do not describe a straight line but a

mixture of at least two lines, one with a large slope ("low affinity") and one with a smaller slope ("high affinity"). This dual affinity behavior is clearly visible in Figure 7C, where the horizontal scale has been changed between 25 μM and 50 μM.

In plant physiology, graphs similar to Figure 7C are usually interpreted as evidence for the presence of two independent uptake systems, one with a "high affinity" and one with a "low affinity" [9]. But here in Figure 7, all data represent the features of a K^+ uptake channel that is widely equated with a "low affinity" transporter, although rare reports present deviating opinions [36].

To understand better potential reasons for this apparent contradiction, the *in-silico* experiment was repeated but the samples were measured at later time points $t_2 > t_1$ (Figure 8A) and $t_3 > t_2$ (Figure 8B). Surprisingly, the apparent "high affinity" component diminishes with increasing time span between start of K^+ uptake and sampling. In Figure 8B, only a "low affinity" component is observable. Please also note that the K_m values are different at the different time points.

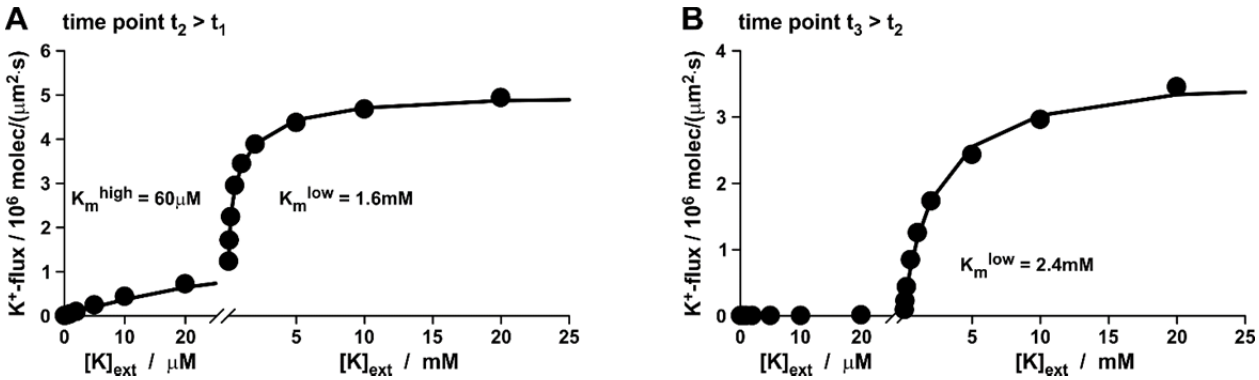

Figure 8. Disappearance of dual affinity with increasing delay between the start of the experiment and the sampling time point. (A) Rate of K^+ absorption as a function of $[K]_{ext}$ measured at a time point $t_2 > t_1$ displayed as in Figure 7A for two ranges. (B) Rate of K^+ absorption as a function of $[K]_{ext}$ measured at a time point $t_3 > t_2$ displayed for two ranges. Lines represent best fits of the data with eqn. 3.2.2.

The reason of the phenomenon of time-dependent affinity is rather simple and best explained in an illustration (Figure 9). In all uptake experiments the internal K^+ concentration increases with time and reaches a saturation level that depends on the (constant) external K^+ concentration. At a lower external K^+ concentration the saturation level is reached earlier than at a higher $[K]_{ext}$. The measured K^+-flux is $\frac{d[K]_{int}}{dt}$ and thus the slope of the $[K]_{int}(t)$-curve at the sampling time point t. If the sampling is very early after the onset of the experiment, also at very low $[K]_{ext}$-values there is still an influx of potassium. However, if the sampling time point is later, the equilibrium between $[K]_{int}$ and $[K]_{ext}$ has been established already for low $[K]_{ext}$ but not for higher $[K]_{ext}$. Consequently, for low $[K]_{ext}$ the slope of the $[K]_{int}(t)$-curve is almost zero at the sampling time point, which means that there is no potassium flux anymore.

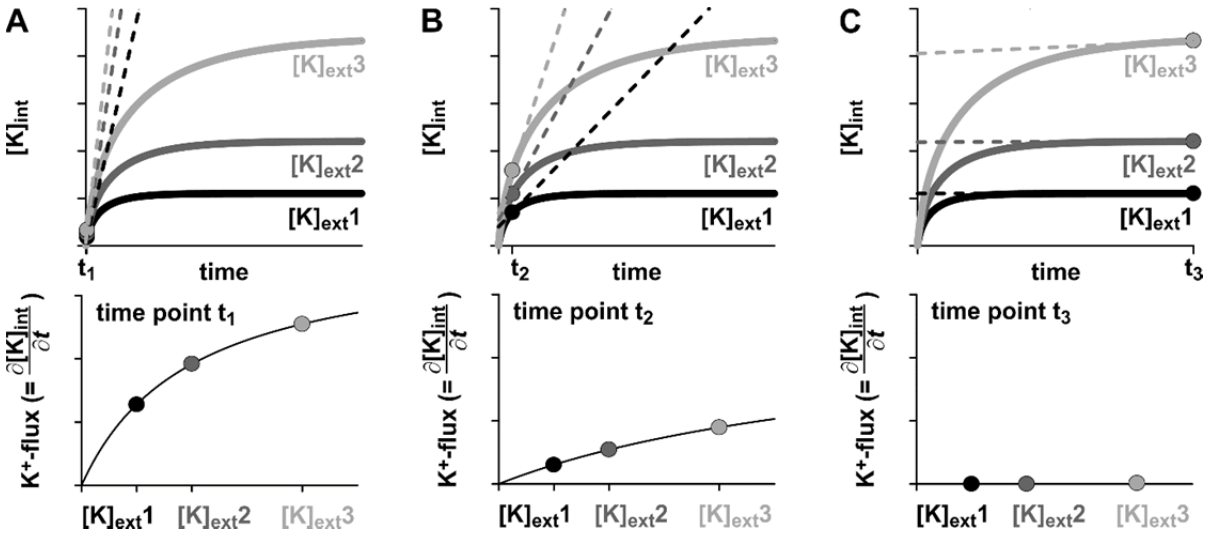

Figure 9. Explanation of the disappearance of dual affinity with increasing delay between the start of the experiment and sampling time point. (Top panels) Time course of the internal K^+ concentration ($[K]_{int}$) for three different external K^+ concentrations ($[K]_{ext}1 < [K]_{ext}2 < [K]_{ext}3$). The flux is measured at the three different time points t_1 (A), t_2 (B), and t_3 (C). The flux is the slope of the $[K]_{int}(t)$-curve at the respective time point. The slopes of the three different curves are shown as dashed lines and cross-referenced by the different grey scales. (Bottom panels) Dependence of the slope (K^+ flux) on the external K^+ concentration at the different time points t_1 (A), t_2 (B), and t_3 (C).

The effect of fast saturation of $[K]_{int}$ and thus the decay of the "high-affinity"-component is sped up by a higher K^+ channel density and/or a higher activity of the H^+-ATPase (Figure 6). Furthermore, it is stronger pronounced in small cells (e.g. yeast) than in larger cells (e.g. *Xenopus* oocytes). The larger the conductance of a channel is or the higher the channel is expressed in the cell, the more difficult is the resolution of its apparent "high affinity" component. In practical terms, it is very likely that in most wet-laboratory experiments characterizing K^+ channels, the channel cord conductance was too big to enable the resolution of the apparent "high affinity" component. The faster a transporter allows the cell to reach the equilibrium, the more difficult it is to find the appropriate experimental conditions, in which the dual affinity behavior can be observed. Consequently, the channels were historically assigned a "low affinity" component, only.

3.3. Do the results and conclusions depend of the exact shape of the current-voltage curves of the transporters?

Qualitatively, the same results are obtained with different shapes of the current-voltage curves of the H^+-ATPase and the potassium channel. Therefore, the exact modeling of these characteristics is not crucial. The H^+-ATPase will always show an S-type curve that intersects the voltage axis at a voltage V_{rev} (V_{rev} varies with the cellular conditions). The bending of the curve does not influence the results qualitatively. Likewise, K^+ channels will always show monotonic increasing current voltage curves that intersect the voltage-axis at V_{rev}. Also here, the bending of these curves does not influence the results qualitatively. Thus, although all conclusions here were drawn from

computational simulations, these simulations cover the broad natural variety and allow the generalization of the results even to "real" potassium channels.

4. Conclusions

The intention of this study is to illustrate the power of computational cell biology for the understanding of plant physiological processes. It is shown that

- Transmembrane transport processes can relatively easy be described by simple mathematical equations, which that are based on fundamental thermodynamic rules.
- Many parameters that are analyzed to characterize channels or transporters (e.g. single-channel conductance) are not needed to know for computational cell biology. Together with others they form a pool of redundant parameters that can be combined.
- The application of the concept of "affinity" to discriminate between "high affinity" and "low affinity" transport processes in plant physiology is not only largely misleading, but is also, from a biophysical point of view, fundamentally wrong.
- K_m and v_{max} values that are often reported to characterize channels/transporters are rather meaningless. They reflect more the conditions of the entire system and the experimental procedure (e.g. the sampling time point) rather than being a characteristic of the transporter.

In summary, the results presented here are a first step towards the demystification of the fairy tale of "high and low affinity" transporters.

Acknowledgements

This work was supported by the FONDECYT grant N 1150054 of the Comisión Nacional Científica y Tecnológica of Chile.

Conflicts of Interest

The author declares no conflicts of interest in this paper.

References

1. G. Volkov A, B. Shtessel Y (2016) Propagation of electrotonic potentials in plants: Experimental study and mathematical modeling. *AIMS Biophys* 3: 358–379.
2. Hedrich R, Salvador-Recatalà V, Dreyer I (2016) Electrical wiring and long-distance plant communication. *Trends Plant Sci* 21: 376–387.
3. Jane Beilby M, Al Khazaaly S (2016) Re-modeling *Chara* action potential: I. from Thiel model of Ca^{2+} transient to action potential form. *AIMS Biophys* 3: 431–449.
4. Hills A, Chen ZH, Amtmann A, et al. (2012) OnGuard, a computational platform for quantitative kinetic modeling of guard cell physiology. *Plant Physiol* 159: 1026–1042.
5. Blatt MR, Wang Y, Leonhardt N, et al. (2014) Exploring emergent properties in cellular homeostasis using OnGuard to model K+ and other ion transport in guard cells. *J Plant Physiol* 171: 770–778.

6. Gajdanowicz P, Michard E, Sandmann M, et al. (2011) Potassium (K+) gradients serve as a mobile energy source in plant vascular tissues. *Proc Natl Acad Sci USA* 108: 864–869.
7. Foster KJ, Miklavcic SJ (2015) Toward a biophysical understanding of the salt stress response of individual plant cells. *J Theor Biol* 385: 130–142.
8. Schott S, Valdebenito B, Bustos D, et al. (2016) Cooperation through Competition-Dynamics and Microeconomics of a Minimal Nutrient Trade System in Arbuscular Mycorrhizal Symbiosis. *Front Plant Sci* 7: 912.
9. Epstein E, Rains DW, Elzam OE (1963) Resolution of dual mechanisms of potassium absorption by barley roots. *Proc Natl Acad Sci USA* 49: 684–692.
10. Hille B (2001) *Ion channels of excitable membranes,* 3rd Ed., Sunderland, MA: Sinauer.
11. Gajdanowicz P, Garcia-Mata C, Gonzalez W, et al. (2009) Distinct roles of the last transmembrane domain in controlling Arabidopsis K+ channel activity. *New Phytol* 182: 380–391.
12. Riedelsberger J, Sharma T, Gonzalez W, et al. (2010) Distributed structures underlie gating differences between the K in channel KAT1 and the Kout channel SKOR. *Mol Plant* 3: 236–245.
13. Garcia-Mata C, Wang J, Gajdanowicz P, et al. (2010) A minimal cysteine motif required to activate the SKOR K+ channel of arabidopsis by the reactive oxygen species H2O2. *J Biol Chem* 285: 29286–29294.
14. González W, Riedelsberger J, Morales-Navarro SE, et al. (2012) The pH sensor of the plant K+-uptake channel KAT1 is built from a sensory cloud rather than from single key amino acids. *Biochem J* 442: 57–63.
15. Lefoulon C, Karnik R, Honsbein A, et al. (2014) Voltage-sensor transitions of the inward-rectifying K+ channel kat1 indicate a latching mechanism biased by hydration within the voltage sensor. *Plant Physiol* 166: 960–975.
16. Hedrich R, Bregante M, Dreyer I, et al. (1995) The voltage-dependent potassium-uptake channel of corn coleoptiles has permeation properties different from other K+ channels. *Planta* 197: 193–199.
17. Hedrich R, Moran O, Conti F, et al. (1995) Inward rectifier potassium channels in plants differ from their animal counterparts in response to voltage and channel modulators. *Eur Biophys J* 24: 107–115.
18. Becker D, Dreyer I, Hoth S, et al. (1996) Changes in voltage activation, Cs+ sensitivity, and ion permeability in H5 mutants of the plant K+ channel KAT1. *Proc Natl Acad Sci USA* 93: 8123–8128.
19. Dreyer I, Antunes S, Hoshi T, et al. (1997) Plant K+ channel α-subunits assemble indiscriminately. *Biophys J* 72: 2143–2150.
20. Dietrich P, Dreyer I, Wiesner P, et al. (1998) Cation sensitivity and kinetics of guard-cell potassium channels differ among species. *Planta* 205: 277–287.
21. Dreyer I, Becker D, Bregante M, et al. (1998) Single mutations strongly alter the K+-selective pore of the K(in) channel KAT1. *FEBS Lett* 430: 370–376.
22. Brüggemann L, Dietrich P, Dreyer I, et al. (1999) Pronounced differences between the native K+ channels and KAT1 and KST1 alpha-subunit homomers of guard cells. *Planta* 207: 370–376.
23. Dreyer I, Michard E, Lacombe B, et al. (2001) A plant Shaker-like K+ channel switches between two distinct gating modes resulting in either inward-rectifying or “leak” current. *FEBS Lett* 505: 233–239.

24. Michard E, Lacombe B, Porée F, et al. (2005) A unique voltage sensor sensitizes the potassium channel AKT2 to phosphoregulation. *J Gen Physiol* 126: 605–617.
25. Michard E, Dreyer I, Lacombe B, et al. (2005) Inward rectification of the AKT2 channel abolished by voltage-dependent phosphorylation. *Plant J* 44: 783–797.
26. Xicluna J, Lacombe B, Dreyer I, et al. (2007) Increased functional diversity of plant K+ channels by preferential heteromerization of the Shaker-like subunits AKT2 and KAT2. *J Biol Chem* 282: 486–494.
27. Geiger D, Becker D, Vosloh D, et al. (2009) Heteromeric AtKC1·AKT1 channels in Arabidopsis roots facilitate growth under K+-limiting conditions. *J Biol Chem* 284: 21288–21295.
28. Held K, Pascaud F, Eckert C, et al. (2011) Calcium-dependent modulation and plasma membrane targeting of the AKT2 potassium channel by the CBL4/CIPK6 calcium sensor/protein kinase complex. *Cell Res* 21: 1116–1130.
29. Garriga M, Raddatz N, Véry AA, et al. (2017) Cloning and functional characterization of HKT1 and AKT1 genes of Fragaria spp.—Relationship to plant response to salt stress. *J Plant Physiol* 210: 9–17.
30. Dreyer I, Müller-Röber B, Köhler B (2004) Voltage gated ion channels, Blatt MR, *Annual Plant Reviews, Membrane Transport in Plants*, Oxford: Blackwell Publishing, 150–192.
31. Eyring H (1935) The activated complex in chemical reactions. *J Chem Phys* 3: 107.
32. Dreyer I, Blatt MR (2009) What makes a gate? The ins and outs of Kv-like K+ channels in plants. *Trends Plant Sci* 14: 383–390.
33. Sharma T, Dreyer I, Riedelsberger J (2013) The role of K(+) channels in uptake and redistribution of potassium in the model plant Arabidopsis thaliana. *Front Plant Sci* 4: 224.
34. Sharma T, Dreyer I, Kochian L, et al. (2016) The ALMT family of organic acid transporters in plants and their involvement in detoxification and nutrient security. *Front Plant Sci* 7: 1488.
35. Loew LM, Schaff JC (2001) The Virtual Cell: a software environment for computational cell biology. *Trends Biotechnol* 19: 401–406.
36. Brüggemann L, Dietrich P, Becker D, et al. (1999) Channel-mediated high-affinity K+ uptake into guard cells from Arabidopsis. *Proc Natl Acad Sci USA* 96: 3298–3302.

AIMS Press